

# Probing the nature of the electroweak phase transition from particle colliders to gravitational wave detectors

Fa Peng Huang<sup>1</sup>, Youping Wan<sup>1</sup>, Dong-Gang Wang<sup>2</sup>, Yi-Fu Cai<sup>2</sup>, and Xinmin Zhang<sup>1</sup>

<sup>1</sup>Theoretical Physics Division, Institute of High Energy Physics,  
Chinese Academy of Sciences, P.O.Box 918-4, Beijing 100049, P.R.China and

<sup>2</sup>CAS Key Laboratory for Researches in Galaxies and Cosmology,  
Department of Astronomy, University of Science and Technology of China,  
Chinese Academy of Sciences, Hefei, Anhui 230026, China

In this letter, we explore the nature of the electroweak phase transition (EWPT) with both particle colliders and gravitational wave (GW) detection. With the observed Higgs mass, the shape of the Higgs potential is fully determined within the standard model (SM) of particle physics. However, it could be changed if there exists new physics beyond the SM. Working with the effective field theory, we show that a modified Higgs potential with a sextic term included can keep the observed 125 GeV Higgs mass but behave different when compared with the SM case. Furthermore, this potential can produce a strong first order phase transition (SFOPT) for the electroweak baryogenesis and interestingly predict new phenomena in the Higgs sector, which can be tested at colliders such as the Large Hadron Collider (LHC) and the planning Circular Electron Positron Collider (CEPC). We point out this SFOPT can lead to detectable signals for the GW interferometers, such as eLISA, DECIGO and BBO. Our present study on the EWPT bridges the particle physics at colliders with the astrophysics and cosmology in the early universe.

*Introduction.*— One scientific target in fundamental physics after the discovery of the Higgs boson [1, 2] is to explore the nature of the electroweak phase transition (EWPT) [3, 4]. This issue is closely related to the details of the Higgs potential beyond the standard model (SM) of particle physics. So far the current data from particle colliders can only provide us with very limited information about the Higgs potential. Except for the quadratic oscillations around the vacuum expectation value (vev)  $v$  which has determined the 125 GeV mass, our knowledge about the Higgs potential remains scarce. For example, without the help of new observational approaches, we cannot tell whether the Higgs potential in reality may be  $V_{\text{tree}}(h) = \frac{1}{2}\mu^2 h^2 + \frac{\lambda}{4}h^4 + \frac{\kappa}{8\Lambda^2}h^6$  rather than the regular case  $V_{\text{tree}}(h) = \frac{1}{2}\mu^2 h^2 + \frac{\lambda}{4}h^4$  in the SM, as sketched in Fig. 1.

Theoretically, the Higgs scenario including a sextic term has been shown to produce the strong first order phase transition (SFOPT) for EW baryogenesis [5–19]. In this Letter we study new predictions of this model for

collider physics and gravitational wave (GW) detection. Our results show that new physics associated with the modified trilinear Higgs coupling can be tested at the LHC and CEPC [20]. Furthermore, associated with the SFOPT, large anisotropic fluctuations can be produced in the stress-energy tensor and hence lead to unique patterns in GW spectra [21–25], which can be detected in the GW detectors, such as eLISA [26], DECIGO [27–29] and BBO [30].

*The effective potential and Collider signals of EWPT*— To investigate the EWPT, we begin with the following tree-level Higgs potential [13, 20]:

$$V_{\text{tree}}(h) = \frac{1}{2}\mu^2 h^2 + \frac{\lambda}{4}h^4 + \frac{\kappa}{8\Lambda^2}h^6. \quad (1)$$

Accordingly, the finite-temperature effective potential up to one-loop level can be written as  $V_{\text{eff}}(h, T) = V_{\text{tree}}(h) + V_1^{T=0}(h) + \Delta V_1^{T \neq 0}(h, T)$  [31], where  $V_1^{T=0}(h)$  is the one-loop Coleman-Weinberg potential at  $T = 0$ , and  $\Delta V_1^{T \neq 0}(h)$  is the thermal contribution with the daisy resummation. In our case, the dominant contribution for the EWPT is from the tree-level barrier, and accordingly, the effective potential with finite temperature effects is approximated as  $V_{\text{eff}}(h, T) \approx \frac{\kappa}{8\Lambda^2}h^6 + \frac{\lambda}{4}h^4 + \frac{1}{2}(\mu^2 + cT^2)h^2$ , with  $c = \frac{1}{16}(-12\frac{\kappa v^2}{\Lambda^2} + g'^2 + 3g^2 + 4y_t^2 + 4\frac{m_h^2}{v^2})$ .<sup>1</sup> The complete one-loop effective potential was given in Ref. [6]. To fix the observed Higgs mass  $m_h = 125$  GeV and the vev  $v$ , the model parameters  $\lambda$  and  $\mu^2$  are shifted

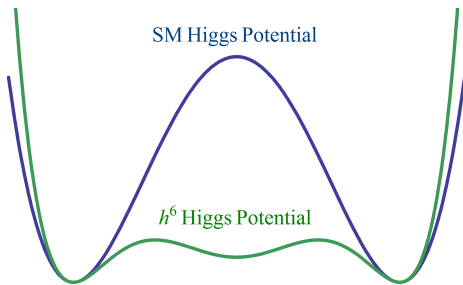


FIG. 1: Sketch of different Higgs potentials. The  $h^6$  potential can realize a process of strong first order EWPT.

<sup>1</sup> The coefficients  $g'$  and  $g$  are the  $U(1)_Y$  and  $SU(2)_L$  gauge couplings, respectively, and  $y_t$  is the top quark Yukawa coupling in the SM.

to:  $\lambda = \lambda_{\text{SM}}(1 - \frac{\Lambda_{\text{max}}^2}{\Lambda^2})$  and  $\mu^2 = \mu_{\text{SM}}^2(1 - \frac{\Lambda_{\text{max}}^2}{2\Lambda^2})$ , with  $\Lambda_{\text{max}} \equiv \sqrt{3\kappa v^2}/m_h$ .

Following the standard analysis of the EWPT/baryogenesis, the critical temperature  $T_c$  and the washout parameter  $v(T_c)/T_c$  are approximated as follows,

$$T_c = \frac{\sqrt{\lambda^2 \Lambda^2 - 4\kappa \mu^2}}{2\sqrt{c\kappa}}, \quad \frac{v(T_c)}{T_c} = \frac{2\Lambda\sqrt{-c\lambda}}{\sqrt{\lambda^2 \Lambda^2 - 4\kappa \mu^2}}. \quad (2)$$

$T_c > 0$  gives a lower bound  $\Lambda_{\text{min}} \equiv \Lambda_{\text{max}}/\sqrt{3} = \sqrt{\kappa}v^2/m_h$ . For  $m_h = 125$  GeV, one gets  $\Lambda_{\text{min}} \approx 480\sqrt{\kappa}$  GeV. One also expects  $\mu^2 + cT^2 > 0$  to stabilize the false vacuum,  $\lambda < 0$  to produce a tree-level potential barrier, and then a positive  $h^6$  term to stabilize the true vacuum. Therefore, the negative  $\lambda$  can yield an upper bound on  $\Lambda$ , namely,  $\Lambda < \Lambda_{\text{max}} \approx 840\sqrt{\kappa}$  GeV. In addition, from the requirement of perturbativity,  $\kappa < 4\pi$ . If one chooses a larger  $\kappa$ , however, a larger bound  $\Lambda_{\text{max}}$  may be achieved. For  $480 \text{ GeV} < \Lambda/\sqrt{\kappa} < 840 \text{ GeV}$ , the washout factor  $v(T_c)/T_c$  is larger than one, which means the SFOPt can be achieved.

An interesting consequence is that the requirement of the SFOPt can lead to an obvious modification of the trilinear Higgs coupling as  $\mathcal{L}_{hhh} = -\frac{1}{6}(1 + \delta_h)A_h h^3$ , with  $A_h = 3m_h^2/v$  being the trilinear Higgs coupling in the SM and  $\delta_h = 2\Lambda_{\text{min}}^2/\Lambda^2$ . In our model  $\delta_h$  varies from 2/3 to 2. Based on this property, we can test this EWPT scenario by measuring the deviation of the trilinear Higgs coupling at the colliders. For the LHC, the deviation of the trilinear Higgs coupling leads to different invariant mass distribution of the Higgs boson pair from the SM case. Due to the challenge of suppressing the large backgrounds at the hadron colliders, the trilinear Higgs coupling is difficult to be completely pinned down at the 14 TeV LHC. However, at the lepton colliders, such as the International Linear Collider(ILC) and CEPC, the trilinear Higgs coupling could be measured precisely.

At the CEPC with  $\sqrt{s} = 240$  GeV, the dominant one-loop contribution to  $hZ$  cross section ( $\sigma_{hZ}$ ) beyond the SM is given by the modified trilinear Higgs coupling [20], which leads to the deviation of  $\sigma_{hZ}$  [20]. Such a deviation is defined as:  $\delta_{\sigma_{hZ}} \equiv \sigma_{hZ}/\sigma_{hZ}^{\text{SM}} - 1$ , which is approximately proportional to  $\delta_h$  as  $\delta_{\sigma_{hZ}} \simeq 1.6\% \delta_h$  at  $\sqrt{s} = 240$  GeV. Thus, for  $\kappa = 1$ , one gets  $\delta_{\sigma_{hZ}} \simeq 7514.17 \text{ GeV}^2/\Lambda^2$ . For the future CEPC with an integrated luminosity of  $10 \text{ ab}^{-1}$ , the precision of  $\sigma_{hZ}$  can be 0.4% [32], which corresponds to  $|\delta_h| \sim 25\%$  [20]. In our scenario,  $\delta_h \in (2/3, 2)$ , and hence, the associated signals are of observable interest at the CEPC.

*GW signals of EWPT.*— For the first order EWPT, there exists a potential barrier between the metastable false vacuum and the true one. When the EWPT is strong enough, true vacuum bubbles are nucleated via quantum tunneling. The temperature goes down with the expansion of the universe, and the nucleation probability

of one bubble per one horizon volume becomes larger and larger. The EWPT completes when the probability is of  $\mathcal{O}(1)$  at the transition temperature, i.e.,  $\Gamma(T_*) \simeq H_*^4$ , and then, we obtain  $S_3(T_*)/T_* = 4 \ln(T_*/100 \text{ GeV}) + 137$ , in which  $S_3 \equiv \int d^3r \left[ \frac{1}{2}(\vec{\nabla}h)^2 + V_{\text{eff}}(h, T) \right]$  is the three dimensional Euclidean action.

The properties of the EWPT and of the bubbles are determined by two key parameters  $\alpha$  and  $\beta$ . Note that,  $\alpha$  is defined by  $\alpha \equiv \frac{\epsilon(T_*)}{\rho_{\text{rad}}(T_*)}$  at the transition temperature  $T_*$ , which depicts the ratio of the false vacuum energy density  $\epsilon(T)$  (the latent heat where  $\epsilon(T_*) = [T \frac{dV_{\text{eff}}^{\text{min}}}{dT} - V_{\text{eff}}^{\text{min}}(T)]|_{T=T_*}$ ) to the plasma thermal energy density  $\rho_{\text{rad}}(T)$  (which is equal to  $\frac{\pi^2}{30}g_*(T)T^4$ ) in the symmetric phase. Moreover, one has  $\beta \equiv -\frac{dS_E}{dt}\bigg|_{t=t_*} \simeq \frac{1}{\Gamma} \frac{d\Gamma}{dt}\bigg|_{t=t_*}$ , where  $S_E(T) \simeq S_3(T)/T$ , and  $\Gamma = \Gamma_0(T) \exp[-S_E(T)]$  represents the variation of the bubble nucleation rate with  $\Gamma_0(T) \propto T^4$ . The parameter  $\alpha$  gives a measure of the strength of the EWPT, namely, a larger value for  $\alpha$  corresponds to a stronger EWPT. Furthermore,  $\beta^{-1}$  corresponds to the typical time scale of the EWPT and its product with the bubble wall velocity  $\beta^{-1}v_b(\alpha)$  represents the size of the bubble.

The collisions of the Higgs vacuum bubbles and their turbulence with plasma are the two distinct mechanisms to generate the stochastic GW. The peak frequency produced by bubble collisions is given by

$$f_{\text{co}} \simeq 5.2 \times 10^{-6} \left( \frac{\beta}{H_*} \right) \left( \frac{T_*}{100 \text{ GeV}} \right) \left( \frac{g_*^t}{100} \right)^{1/6} \text{ Hz},$$

and the corresponding GW intensity is calculated as

$$\Omega_{\text{co}}(f_{\text{co}})h^2 \simeq c\varepsilon^2 \left( \frac{H_*}{\beta} \right)^2 \left( \frac{\alpha}{1 + \alpha} \right)^2 \left( \frac{v_b^3}{0.24 + v_b^3} \right) \left( \frac{100}{g_*^t} \right)^{\frac{1}{3}},$$

with  $c = 1.1 \times 10^{-6}$  [33]. The coefficient  $\varepsilon$  (which characterizes the fraction of the latent heat that is transformed to the fluid kinetic energy), the bubble velocity  $v_b$  and the turbulent fluid velocity  $u_s$  are functions of  $\alpha$  [34]. Here,  $g_*^t (= g_*(T_*))$  is the total number of degrees of freedom at  $T_*$ . It is interesting to notice that, in the low frequency regime the spectrum  $\Omega_{\text{co}}(f)h^2$  increases as  $f^{2.8}$ , but in the high frequency regime it decreases as  $f^{-1}$  [35]. In this regard, the EWPT has predicted particular patterns of the intensity spectrum which could be observational signals in GW surveys.

On the other side, the GW signals produced by the turbulence interaction has a peak frequency at about

$$f_{\text{tu}} \simeq 3.4 \times 10^{-6} \frac{u_s}{v_b} \left( \frac{\beta}{H_*} \right) \left( \frac{T_*}{100 \text{ GeV}} \right) \left( \frac{g_*^t}{100} \right)^{1/6} \text{ Hz},$$

with the intensity

$$\Omega_{\text{tu}}(f_{\text{tu}})h^2 \simeq 1.4 \times 10^{-4} u_s^5 v_b^2 \left( \frac{H_*}{\beta} \right)^2 \left( \frac{100}{g_*^t} \right)^{1/3}.$$

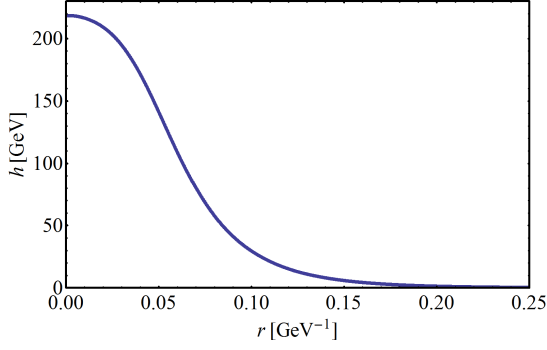


FIG. 2: The Higgs bubble profile for  $\kappa = 1$ ,  $T = 51.94$  GeV and  $\Lambda = 600$  GeV.

Again, in the low frequency regime the spectrum  $\Omega_{\text{tu}}(f)h^2$  increased as  $f^2$ , but in the high frequency regime it decreased as  $f^{-3.5}$  [33].

The two characteristic parameters  $\alpha$  and  $\beta$  can be evaluated by solving the Higgs bubble profile from the following equation

$$\frac{d^2 h}{dr^2} + \frac{2}{r} \frac{dh}{dr} = \frac{\partial V_{\text{eff}}}{\partial h},$$

with the boundary conditions  $h(r \rightarrow \infty) = 0$ ,  $\frac{dh(r=0)}{dr} = 0$ . Using the overshoot/undershoot method, one can numerically determine the exact profile of the Higgs bubble after fixing the model parameters  $\kappa$  and  $\Lambda$ . As a demonstration, we present one numerical solution in Fig. 2 for the specific case of  $\kappa = 1$  and  $\Lambda = 600$  GeV. It is worth noting that, however, the bubble wall runs away if  $\Lambda$  becomes smaller than 590 GeV [36, 37]. Once the Higgs profile has been found, all associated parameters can be derived, and accordingly, the predicted GW spectra can be calculated such as shown in Fig. 3.

*Results and Discussions.*— In Fig. 3, the GW spectra  $h^2\Omega_{\text{GW}}$  and the  $hZ$  cross section deviations  $\delta_{\sigma_{hZ}}$  are presented by taking different values of the cutoff scale  $\Lambda$  (590 GeV, 600 GeV, 650 GeV and 700 GeV) with  $\kappa$  being fixed to unity in the Higgs scenario under consideration. For instance, the red curve in the figure depicts the GW signals for  $\Lambda = 590$  GeV predicted by our model, which also predicts a collider signature of the cross section deviation  $\delta_{\sigma_{hZ}} \simeq 2.2\%$  (the corresponding deviation of the trilinear Higgs coupling  $\delta_h$  is 1.32) which is expected to be tested at the CEPC. In addition, we numerically present the theoretical curves for the cases of 600 GeV, 650 GeV and 700 GeV, as shown by the blue, green and black lines, respectively. These curves correspond respectively to the values of 2.1%, 1.8%, and 1.5% for  $\delta_{\sigma_{hZ}}$ .

From our result, it is obvious that the amplitude of the GW spectrum is more significant for smaller cutoff scales. This fact can be naturally explained by the observation that in Eq. (1) a smaller  $\Lambda$  yields a larger contribution of the sextic operator which then leads to a stronger EWPT. Moreover, it can be found that the GW signals are peaked

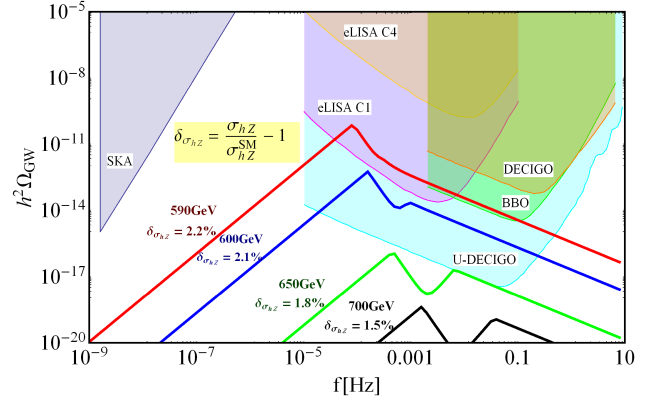


FIG. 3: GW spectra  $h^2\Omega_{\text{GW}}$  and the  $hZ$  cross section deviations  $\delta_{\sigma_{hZ}}$  for different cutoff scales  $\Lambda$  (590 GeV, 600 GeV, 650 GeV and 700 GeV) with  $\kappa = 1$  in our Higgs model. The colored regions show the expected experimental sensitivities of future GW interferometers for eLISA, DECIGO, BBO, U-DECIGO, and SKA. The red line depicts the GW signal for  $\Lambda = 590$  GeV, which also gives rise to a collider signal of  $\delta_{\sigma_{hZ}} \simeq 2.2\%$  at the CEPC. The blue, green and black lines are the cases for 600 GeV, 650 GeV and 700 GeV, respectively.

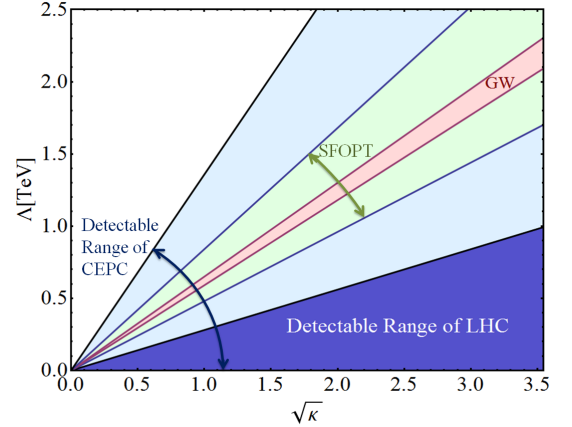


FIG. 4: The observational abilities of different experiments. For CEPC, the sensitive region is  $\Lambda/\sqrt{\kappa} < 1357.65$  GeV; for LHC, it corresponds to  $\Lambda/\sqrt{\kappa} < 280$  GeV; the theoretical condition for the SFOPT requires  $480 \text{ GeV} < \Lambda/\sqrt{\kappa} < 840 \text{ GeV}$ ; and the detectable region of GW interferometers reads  $590 \text{ GeV} < \Lambda/\sqrt{\kappa} < 650 \text{ GeV}$ .

around  $10^{-4}$  Hz, which lies in the detectable range of satellite based GW experiments. The colored regions in Fig. 3 show the expected experimental sensitivities of future GW interferometers including eLISA<sup>2</sup> [38], SKA, BBO, DECIGO [39] and Ultimate-DECIGO (U-DECIGO) [40].

<sup>2</sup> The eLISA C1 and C4 in the figure are two representative configurations studied in Ref. [38].

From Fig. 3, one can explicitly see that eLISA, BBO and U-DECIGO are all capable of detecting the GW signals generated from the EWPT at low cutoff scales described by our model.

As a result, the collider experiments in particle physics and the GW experiments are naturally related to each other through the exploration of the nature of the EWPT, i.e. there is a strong correlation between the strength of the GWs and the deviation of the trilinear Higgs coupling. As shown in Fig. 3, each lines relates the GW signals to the associated collider signals with the same cutoff scale. To obtain a global picture of this correlation, we present the observational abilities of different experiments in Fig. 4. For the CEPC with  $\sqrt{s} = 240$  GeV, the sensitive region is  $\Lambda/\sqrt{\kappa} < 1357.65$  GeV; for LHC, it corresponds to  $\Lambda/\sqrt{\kappa} < 280$  GeV; the theoretical condition for the SFOPt roughly requires  $480 \text{ GeV} < \Lambda/\sqrt{\kappa} < 840 \text{ GeV}$ ; and the detectable region of GW interferometers reads  $590 \text{ GeV} < \Lambda/\sqrt{\kappa} < 650 \text{ GeV}$ .

Consequently, we can find that, in order to probe the physics of the EWPT, the detectable ability of the LHC is weak, but the future CEPC and the GW detections are very promising in precisely detecting or even measuring the predicted signals. For example, for the cutoff scale  $\Lambda = 590$  GeV, the deviation of the trilinear Higgs coupling is 1.32, which can not be tested at the LHC. However, the GW experiments could indirectly measure this trilinear Higgs coupling, which corresponds to the red line in Fig.3. We conclude that the GW interferometers can provide a complementary approach to explore the nature of the EWPT beyond terrestrial colliders, and vice versa.

*Conclusion*— After the discovery of the 125 GeV Higgs boson, it becomes a urgent problem to unravel the nature of the EWPT. If the EWPT is a strong first order process, it will naturally relate to the mechanism of the spontaneous symmetry breaking, the EW baryogenesis and the GW physics. We have studied the EWPT in the framework of effective field theory and investigated its predicted signals at colliders, i.e., the deviation of the trilinear Higgs coupling from the SM. Moreover, we put forward a complementary approach to exploring the nature of the EWPT by analyzing its GW signals generated in the early universe. From our calculation the GW spectrum produced via the bubble collisions and the turbulence with the plasma during the first order EWPT can be significant enough to be detected by the forthcoming GW experiments. The study performed in this Letter will help us to deeply understand the nature of the EWPT, which may open a new window in the particle physics, and it highlights the interactions between particle physics and cosmology.

*Acknowledgements*.— FPH, YPW and XZ are supported in part by the NSFC (Grant Nos. 11121092, 11033005, 11375220) and by the CAS pilotB program. DGW and YFC are supported in part by the Chinese National Youth Thousand Talents Program, by the USTC

start-up funding (Grant No. KY2030000049) and by the NSFC (Grant No. 11421303). The operation of this super-computation is funded by the particle cosmology group at USTC.

- 
- [1] G. Aad *et al.* [ATLAS Collaboration], Phys. Lett. B **716**, 1 (2012) [arXiv:1207.7214 [hep-ex]].
  - [2] S. Chatrchyan *et al.* [CMS Collaboration], Phys. Lett. B **716**, 30 (2012) [arXiv:1207.7235 [hep-ex]].
  - [3] CEPC-SPPC Study Group, IHEP-CEPC-DR-2015-01, IHEP-TH-2015-01, HEP-EP-2015-01.
  - [4] N. Arkani-Hamed, T. Han, M. Mangano and L. T. Wang, arXiv:1511.06495 [hep-ph].
  - [5] C. Grojean and G. Servant, Phys. Rev. D **75**, 043507 (2007) [hep-ph/0607107].
  - [6] C. Delaunay, C. Grojean and J. D. Wells, JHEP **0804**, 029 (2008) [arXiv:0711.2511 [hep-ph]].
  - [7] S. J. Huber and T. Konstandin, JCAP **0805**, 017 (2008) [arXiv:0709.2091 [hep-ph]].
  - [8] S. Das, P. J. Fox, A. Kumar and N. Weiner, JHEP **1011**, 108 (2010) [arXiv:0910.1262 [hep-ph]].
  - [9] J. R. Espinosa, T. Konstandin, J. M. No and M. Quiros, Phys. Rev. D **78**, 123528 (2008) [arXiv:0809.3215 [hep-ph]].
  - [10] M. Jarvinen, C. Kouvaris and F. Sannino, Phys. Rev. D **81**, 064027 (2010) [arXiv:0911.4096 [hep-ph]].
  - [11] J. R. Espinosa, T. Konstandin, J. M. No and G. Servant, JCAP **1006**, 028 (2010) [arXiv:1004.4187 [hep-ph]].
  - [12] M. Kakizaki, S. Kanemura and T. Matsui, Phys. Rev. D **92**, 115007 (2015) [arXiv:1509.08394 [hep-ph]].
  - [13] X. m. Zhang, Phys. Rev. D **47**, 3065 (1993) [hep-ph/9301277].
  - [14] X. Zhang and B. L. Young, Phys. Rev. D **49**, 563 (1994) [hep-ph/9309269].
  - [15] X. Zhang, B. L. Young and S. K. Lee, Phys. Rev. D **51**, 5327 (1995) [hep-ph/9406322].
  - [16] X. Zhang, S. K. Lee, K. Whisnant and B. L. Young, Phys. Rev. D **50**, 7042 (1994) [hep-ph/9407259].
  - [17] K. Whisnant, B. L. Young and X. Zhang, Phys. Rev. D **52**, 3115 (1995) [hep-ph/9410369].
  - [18] B. Grzadkowski, J. Pliszka and J. Wudka, Phys. Rev. D **69**, 033001 (2004) [hep-ph/0307338].
  - [19] F. P. Huang and C. S. Li, Phys. Rev. D **92**, 075014 (2015) [arXiv:1507.08168 [hep-ph]].
  - [20] F. P. Huang, P. H. Gu, P. F. Yin, Z. H. Yu and X. Zhang, arXiv:1511.03969 [hep-ph].
  - [21] E. Witten, Phys. Rev. D **30**, 272 (1984).
  - [22] C. J. Hogan, Phys. Lett. B **133**, 172 (1983).
  - [23] C. J. Hogan, Mon. Not. Roy. Astron. Soc. **218**, 629 (1986).
  - [24] M. S. Turner and F. Wilczek, Phys. Rev. Lett. **65**, 3080 (1990).
  - [25] P. Schwaller, Phys. Rev. Lett. **115**, 181101 (2015) [arXiv:1504.07263 [hep-ph]].
  - [26] P. A. Seoane *et al.* [eLISA Collaboration], arXiv:1305.5720 [astro-ph.CO].
  - [27] N. Seto, S. Kawamura and T. Nakamura, Phys. Rev. Lett. **87**, 221103 (2001) [astro-ph/0108011].
  - [28] S. Kawamura *et al.*, Class. Quant. Grav. **23**, S125 (2006).
  - [29] S. Kawamura *et al.*, Class. Quant. Grav. **28**, 094011 (2011).

- [30] V. Corbin and N. J. Cornish, *Class. Quant. Grav.* **23**, 2435 (2006) [gr-qc/0512039].
- [31] M. Quiros, hep-ph/9901312.
- [32] M. Bicer *et al.* [TLEP Design Study Working Group Collaboration], *JHEP* **1401**, 164 (2014) [arXiv:1308.6176 [hep-ex]].
- [33] A. Nicolis, *Class. Quant. Grav.* **21**, L27 (2004) [gr-qc/0303084].
- [34] M. Kamionkowski, A. Kosowsky and M. S. Turner, *Phys. Rev. D* **49**, 2837 (1994) [astro-ph/9310044].
- [35] S. J. Huber and T. Konstandin, *JCAP* **0809**, 022 (2008) [arXiv:0806.1828 [hep-ph]].
- [36] D. Bodeker and G. D. Moore, *JCAP* **0905**, 009 (2009) [arXiv:0903.4099 [hep-ph]].
- [37] S. J. Huber and M. Sopena, arXiv:1302.1044 [hep-ph].
- [38] C. Caprini *et al.*, arXiv:1512.06239 [astro-ph.CO].
- [39] C. J. Moore, R. H. Cole and C. P. L. Berry, *Class. Quant. Grav.* **32**, 015014 (2015) [arXiv:1408.0740 [gr-qc]].
- [40] H. Kudoh, A. Taruya, T. Hiramatsu and Y. Himemoto, *Phys. Rev. D* **73**, 064006 (2006) [gr-qc/0511145].